NASA TECHNICAL NOTE

NASA TN D-7765

NASA TN D-7765

ION HEATING IN A PLASMA FOCUS

by Frank Hohl and S. Peter Gary

Langley Research Center
Hampton, Va. 23665

NATIONAL AERONAUTICS AND SPACE ADMINISTRATION • WASHINGTON, D. C. • NOVEMBER 1974

1. Report No. NASA TN D-7765	2. Government Accession No.	3. Recipient's Catalog No.
4. Title and Subtitle ION HEATING IN A PLASMA FOCUS		5. Report Date November 1974
		6. Performing Organization Code
7. Author(s) Frank Hohl and S. Peter Gary		8. Performing Organization Report No. L-9767
9. Performing Organization Name and Address NASA Langley Research Center Hampton, Va. 23665		10. Work Unit No. 502-10-01-01
		11. Contract or Grant No.
12. Sponsoring Agency Name and Address National Aeronautics and Space Administration Washington, D.C. 20546		13. Type of Report and Period Covered Technical Note
		14. Sponsoring Agency Code

16. Abstract

Ion acceleration and heating in a plasma focus are investigated by the numerical integration of the three-dimensional equations of motion. The electric and magnetic fields given were derived from experimental data. The results obtained show that during the collapse phase of focus formation, ions are efficiently heated to temperatures of several keV. During the phase of rapid current reduction, ions are accelerated to large velocities in the axial direction. The results obtained with the model are in general agreement with experimental results.

17. Key Words (Suggested by Author(s)) Ion heating Plasma focus	18. Distribution Statement Unclassified – Unlimited STAR Category 25

19. Security Classif. (of this report) Unclassified	20. Security Classif. (of this page) Unclassified	21. No. of Pages 28	22. Price* $3.25

ION HEATING IN A PLASMA FOCUS

By Frank Hohl and S. Peter Gary*
Langley Research Center

SUMMARY

Ion acceleration and heating in a plasma focus are investigated by the numerical integration of the three-dimensional equations of motion. The electric and magnetic fields given were derived from experimental data. The results obtained show that during the collapse phase of focus formation, ions are efficiently heated to temperatures of several keV. During the phase of rapid current reduction, ions are accelerated to large velocities in the axial direction. The results obtained with the model are in general agreement with experimental results.

INTRODUCTION

Plasma focus devices (ref. 1) are presently under study in a number of laboratories. When operated with deuterium at pressures of a few hundred pascals (a few torr), the plasma focus emits neutron bursts of 10^9 to 10^{13} neutrons with a neutron production time around 100 ns. Average energy shifts of up to 500 keV, corresponding to center-of-mass velocities up to 2 Mm/s are obtained by analyzing the neutron energies in the axial direction (refs. 2 and 3). In general, the experimental data obtained by the various investigators (refs. 2 to 8) do not fit either of the simple models commonly proposed, namely, the beam-target or moving-boiler models. The experimental observations which a successful model of the plasma focus formation must explain are ion heating to keV temperatures (refs. 3 and 9) and axial ion velocities corresponding to energies of at least 300 keV (refs. 2, 10, and 11).

The two-dimensional fluid model of Potter (ref. 12) describes well the initial phase of focus formation and agrees with a number of the observed properties. Such a model, however, does not include the detailed process of ion and electron heating apparently occurring during the final phase of focus formation. For example, the two-dimensional magnetohydrodynamic simulations are unable to account for the experimentally observed anisotropy in the neutron emission.

Bernstein (ref. 13) has presented a model that more closely represents the experimental data. The present work extends his results but differs in a number of important

---

*Assistant professor, College of William and Mary, Williamsburg, Virginia.

aspects. First, in the present work two variations in the electric field are considered: one resulting from the radial velocity of the collapsing plasma and the other resulting from the rapid current decrease during the final focus formation. Bernstein considered only the electric field induced during the collapsing phase and thus, neglected the important phase of rapid current reduction. Experimentally, this current-reduction phase has been proven to be a characteristic of focus formation.

Also, in his model Bernstein assumed an on-axis electric field of zero; this assumption implies a strong electric field away from the axis, where the magnetic field is strong. This leads to heating, but also prevents ions from acquiring large axial velocities. In the present work, the axial electric field is zero outside the plasma (at the outer electrode), in agreement with Lenz' law. Thus, the strong electric field in the region of low magnetic field near the axis allows strong ion acceleration. Since experimental results indicate a correlation between the rapid current drop and ion acceleration, this phase of focus formation is also investigated in the present work. The present work improves Bernstein's work in several other respects in that it calculates the ion motion in three-dimensional space rather than in two, treats initial distribution with Maxwellian velocity distributions, and considers much larger numbers of ions.

It should be emphasized that the present calculation, like Bernstein's, is not self-consistent. The electric and magnetic fields are assumed as given, and the response of the ions to the fields is calculated. Assuming the fields as given is possible only when the ion response does not significantly affect the fields. Since the electrons are the primary current carriers, this assumption is satisfied for the present work. The present method has the advantage of allowing a fully three-dimensional treatment that includes the effects of strongly inhomogeneous fields. Some initial results of the present work were published elsewhere (ref. 14).

Figure 1 displays a cross section through a plasma focus apparatus, which consists of two coaxial cylindrical electrodes. The outer electrode has an inner diameter of 10 cm and the inner electrode has an outer diameter of 5 cm. Figure 2 shows a streak photograph of the plasma focus formation taken with an image converter camera. The photograph displays a region 0.5 cm above the center electrode viewed through a 0.2-cm-wide slit perpendicular to the axis. The time interval from -50 ns to 0, as shown in figure 2, when the plasma column is in the final collapse phase, is considered the compression phase in the present paper. The time interval from 0 to about 50 ns is the period when maximum compression has occurred, and during this time, a rapid current reduction takes place. This rapid current reduction is illustrated in figure 3, which shows typical oscilloscope traces of the current and induced electric field in the plasma focus apparatus.

Note that because of the relatively slow detector response, the current reduction appears to take place during a time of about 200 ns. However, the electric field induced by the changing current shows that the principal change in the current takes place during a time of the order of 50 ns.

<div align="center">SYMBOLS</div>

$\vec{B}$ magnetic field

$\vec{E}$ electric field

e   magnitude of electronic charge

I   total current

$\vec{j}$ current density

$\vec{j}_o$ current density for the compression phase at $t = 0$

$\vec{j}_1$ current density for the rapid current-reduction phase

m   mass of deuterium ion

r, θ, z cylindrical coordinates

r_c radius of current-carrying region at collapse

r_o initial radius of plasma column for the compression phase

r_1 radius of plasma column at maximum compression

r_2 radius of outer electrode

T   temperature derived from $\frac{1}{2} m \left\langle \left(v - \langle v \rangle \right)^2 \right\rangle$

T^* effective energy of ion beam derived from $\frac{1}{2} m \left\langle \langle v_z \rangle^2 \right\rangle$

t   time

V	velocity
V_c	collapse velocity
x,y,z	rectangular coordinates
β	inverse time constant
μ_o	permeability of free space

Subscripts:

max	maximum
x,y,z	x-, y-, and z-components
θ	azimuthal component

Notation:

$\langle\ \rangle$	root-mean-square value
$\hat{\ }$	unit vector

THE MODEL

The equations describing the motion of deuterium ions subject to electric and magnetic fields are

$$\frac{d\vec{V}(t)}{dt} = \frac{e}{m}\left[\vec{E}(r,t) + \vec{V}(t) \times \vec{B}(r,t)\right] \tag{1}$$

and

$$\frac{d\vec{r}(t)}{dt} = \vec{V}(t) \tag{2}$$

where cylindrical symmetry of the fields is assumed. The electric and magnetic fields are determined from Maxwell's equations

$$\nabla \times \vec{E} = -\frac{\partial\vec{B}}{\partial t} \tag{3}$$

4

and

$$\nabla \times \vec{B} = \mu_0 \vec{j} \tag{4}$$

where μ_0 is the permeability of free space, $\vec{j}$ is the current density, and the displacement current is neglected. The current density is assumed to be azimuthally symmetric along the axis of the plasma focus; that is

$$\vec{j}(r,t) = \hat{z} j_z(t) \tag{5}$$

Thus,

$$\vec{B}(r,t) = \hat{\theta} B_\theta(r,t) \tag{6}$$

and

$$\vec{E}(r,t) = \hat{z} E_z(r,t) \tag{7}$$

Two phases of the current variation in the plasma focus are investigated. The first is that occurring during the compression phase when a circular region of uniform current density is compressed. Nonuniform current densities are not expected to change significantly the results obtained (ref. 13). The second phase of current variation is that which occurs near peak compression and results in a rapid reduction of the total current.

Compression Phase

The final compression phase of plasma focus formation occurs over such a short time interval that the total current can be assumed to remain constant (refs. 1 and 8). Also, the current distribution is assumed to be uniform over a circular region, the edge of which is compressed at a radial velocity V_c of 180 km/s (ref. 15). The radius of the circular region is given by

$$r_c = r_0 - V_c t \tag{8}$$

where r_0 is the initial radius at $t = 0$. Thus, the axial current density distribution is

$$\left. \begin{aligned} j_z(r,t) &= j_0 \frac{r_0^2}{r_c^2} & \left(r \leq r_c(t)\right) \\[2ex] j_z(r,t) &= 0 & \left(r > r_c(t)\right) \end{aligned} \right\} \tag{9}$$

The resulting magnetic field is

$$B_\theta(r,t) = \frac{\mu_0 j_0 r}{2} \frac{r_0^2}{r_c^2} \qquad \left(r \leqq r_c(t)\right)$$

$$B_\theta(r,t) = \frac{\mu_0 j_0 r}{2} \frac{r_0^2}{r^2} \qquad \left(r > r_c(t)\right)$$

$$(10)$$

From Maxwell's equation

$$\frac{\partial E_z}{\partial r} = \frac{\partial B_\theta}{\partial t}$$

the axial component of the electric field is found to be

$$E_z(r,t) = \frac{\mu_0 j_0 V_c r_0^2}{2 r_c^3} \left(r^2 - r_c^2\right) \qquad \left(r \leqq r_c(t)\right)$$

$$E_z(r,t) = 0 \qquad \left(r > r_c(t)\right)$$

$$(11)$$

Rapid Current-Reduction Phase

Near the time of maximum compression, the characteristic current trace for the plasma focus shows a reduction in the total current of the order of 30 percent during a time period about 50 ns. Thus, the current density variation during this time period is

$$j_z(r,t) = j_1(1 - \beta t) \qquad \left(r \leqq r_1\right)$$

$$j_z(r,t) = 0 \qquad \left(r > r_1\right)$$

$$(12)$$

where r_1 is the radius of the plasma column at maximum compression, and $j_1 = I / \pi r_1^2$, where I is the total current through the focus. This current distribution results in a magnetic field given by

$$B_\theta(r,t) = \frac{\mu_0 j_1 r}{2} (1 - \beta t) \qquad \left(r \leqq r_1\right)$$

$$B_\theta(r,t) = \frac{\mu_0 j_1 r_1^2}{2r} (1 - \beta t) \qquad \left(r_2 > r > r_1\right)$$

$$(13)$$

6

The corresponding electric field is

$$E_z(r) = -\frac{\mu_o j_1 \beta}{4}\left(r^2 - 2r_1^2 \ln\frac{r_2}{r_1}\right) \qquad\qquad (r \leqq r_1)$$

$$E_z(r) = -\frac{\mu_o j_1 \beta}{4} r_1^2\left(1 + 2\ln\frac{r}{r_1} - 2\ln\frac{r_2}{r_1}\right) \qquad (r_2 > r > r_1)$$

(14)

The radius r_2, which corresponds to the outer electrode of the plasma focus, is 5 cm for the present investigation. The induced electric field outside r_2 is zero, and this boundary condition is used in deriving equation (14). Note that the electric field given by that equation is time independent, since the current decrease is linear.

RESULTS

The first case considered is the collapse phase of the plasma focus. The magnetic and induced electric fields are given by equations (10) and (11), respectively. The initial radius of the collapsing plasma column r_0 is taken to be 1 cm and the collapse speed of the column V_c is 180 km/s (ref. 15). Also, the total current is 1 MA, so that $j_0 = \frac{1\ \text{MA}}{\pi r_0^2}\left(\frac{10}{\pi}\ \text{GA/m}^2\right)$ in equations (10) and (11). At the beginning of the simulation, the deuterium ions are uniformly distributed over a circular region of radius r_0 and have a Maxwellian velocity distribution corresponding to a temperature of 10 eV (ref. 16). Results obtained with an initial temperature of 100 eV are essentially identical with those presented herein.

Figure 4 shows the variation in the magnetic field at six times during the collapse phase. The magnetic field near the edge of the current-carrying column increases to large values as the column is compressed. Figure 5 shows the corresponding variation in the induced electric field. As can be seen from these two figures, the magnitude of the electric field peaks at the axis ($r = 0$), where the magnetic field is zero. However, since the $\vec{E} \times \vec{B}$ ion drift is radially outward, the condition of a large axial electric field and a low magnetic field cannot be effectively exploited to give large axial ion velocities. This is illustrated in figure 6, which displays the evolution of the spatial ion distribution and shows that the ions are expelled from the central region by the $\vec{E} \times \vec{B}$ drift. Nevertheless, there occurs strong heating for an appreciable portion of the ions, as illustrated in figure 7, which shows the evolution of the transverse ion velocities in V_x-V_y space.

The evolution of the axial velocities as a function of axial position is shown in figure 8. Again, large velocities are acquired by a considerable fraction of the ions, and

at the same time, the ions perform a cyclotron motion which confines them near their original location of $z = 0$. These results are summarized in figure 9, which displays the evolution of various temperature components derived from the rms velocities. In this figure T_{xy} represents the transverse temperature, T_z is the axial component, and T_z^* corresponds to the energy in directed beam motion in the z-direction. As can be seen, a temperature of several keV is obtained as a result of heating due to induced electric fields during the collapse phase. Note also that this heating takes place during the time that the ions are expelled from the central region.

As the $\vec{E} \times \vec{B}$ drift forces the ions from the central region, the mean radius $\langle r \rangle$ of the ion distribution increases from about 7 mm to 8 mm. After 20 ns, the mean radius and the temperature show little further increase. When all the ions are initially confined to a smaller circular region of radius 1 mm, then the mean radius $\langle r \rangle$ increases by a factor of 10, from about 0.7 mm to 7 mm. This is illustrated in figure 10, which shows the evolution of a system identical with that in figure 6, except that now the initial radius of the uniform ion distribution is reduced by a factor of 10. The temperature components calculated for the system in figure 10 are also larger by a factor of 10 than those shown in figure 9. Again, the heating occurs primarily during the initial 20 ns as the ions are expelled from the central region.

The results for the rapid current-reduction phase are presented next. Equations (13) and (14) now give the magnetic and induced electric fields. The current reduction takes place near the time of maximum compression, when the radius of the current-carrying column is about 1 mm. Thus, $j_1 = I/\pi r_1^2$, where $r_1 = 1$ mm and the total current I is 1 MA. The parameter β in equation (12), which is determined in agreement with experimental data to obtain a 30-percent current reduction in 50 ns is 1 Ms^{-1}. The radius r_2 in equation (14) corresponds to the radius of the outer electrode of the plasma focus apparatus and has a value of 5 cm.

The variation in the magnetic field, as given by equation (13), is shown in figure 11 at six times during the current-reduction phase. Figure 12 shows the induced electric field, which remains constant during the current-reduction phase, and figure 13 shows the evolution of the initially uniform ion distribution in x-y space. Since the compression phase, with its strong ion heating, precedes the phase of rapid current decrease, a larger initial temperature of 200 eV was given to the ions. The initial radius of the ion distribution in figure 13 is 1 cm. Note that the $\vec{E} \times \vec{B}$ drift is now radially inward and causes an inward compression of the ions.

In the central region of large electric field and low magnetic field, the ions are rapidly accelerated along the z-axis. At the same time, more ions are pushed toward the axis by the $\vec{E} \times \vec{B}$ drift. Figure 14 summarizes some of these results. The transverse temperature increases by only about a factor of 4, while T_z shows a much larger

increase because new ions continually reach the central region, where they are accelerated along the z-axis, thus producing a large axial velocity spread.

Since most of the acceleration occurs near the axis, an initial ion distribution identical with that shown in figure 13, except that the initial radius was reduced to 1 mm, was investigated. The resulting evolution of the spatial ion distribution is shown in figure 15. Note that during the time interval of 50 ns shown, all the ions are compressed to a small radius. Figure 16 shows a typical ion orbit in both the x-y and the r-z planes. Starting at a radius of about 0.6 mm, the ion begins to spiral inward toward the axis. After reaching a radius of about 0.2 mm, the ion begins to circle the z-axis and at the same time experiences a large acceleration along the z-axis.

Figure 17 shows the evolution of the V_y-V_x distribution of the ions. Since all the ions are now in the region near the axis, they experience a considerable increase in temperature, as shown in figure 18, where these results are summarized. First, it can be seen that the transverse energy of the ions near the axis reaches several keV. At the same time, T_z reaches a value of about 60 keV. The value of T_z shown in figure 18 should not be interpreted as a true temperature, as it results primarily from the different times at which ions reach the central region, where efficient acceleration along the z-axis occurs. Note that after all ions have arrived in this region ($t \approx 20$ ns), T_z no longer increases. The average beam energy of the ions T_z^* reaches very large values in this simulation because all the ions now acquire large velocities along the z-axis.

Since the accelerating region, or current column, in the plasma focus extends only about 3 cm, the acceleration of ions should terminate when z is greater than that value. Figure 19 shows that the fastest ions reach $z = 3$ cm at about $t = 30$ ns, at which time T_z^* is approximately 500 keV (fig. 18). In the actual plasma focus, T_z^* should level off near that value.

CONCLUDING REMARKS

The model presented provides for both ion heating to several keV and ion acceleration in the axial direction to velocities corresponding to an energy of several hundred keV, in agreement with experimental results. The initial collapse phase is the primary ion heating phase, whereas the high axial velocity of the ions is acquired during the phase of rapid current reduction. The fields were determined from experimental data, and the ions moved under the influence of these given fields. Taking the fields as given is justified since the much less massive electrons are the primary current carriers and thus determine the structure of the magnetic and induced electric fields. A more detailed under-

standing of focus formation, such as the cause of the increased resistivity which produces the rapid current drop, will require more involved simulations and analyses.

Langley Research Center,
    National Aeronautics and Space Administration,
        Hampton, Va., September 12, 1974.

REFERENCES

1. Mather, J. W.: Dense Plasma Focus. Plasma Physics. Vol. 9, Pt. B of Methods of Experimental Physics, Ralph H. Lovberg and Hans R. Griem, eds., Academic Press, Inc., 1971, pp. 187-249.

2. Lee, J. H.; Shomo, L. P.; Williams, M. D.; and Hermansdorfer, H.: Neutron Production Mechanism in a Plasma Focus. Phys. Fluids, vol. 14, no. 10, Oct. 1971, pp. 2217-2223.

3. Bernstein, M. J.; Meskan, D. A.; and Van Paassen, H. L. L.: Space, Time, and Energy Distributions of Neutrons and X Rays From a Focused Plasma Discharge. Phys. Fluids, vol. 12, no. 10, Oct. 1969, pp. 2193-2202.

4. Gratreau, P.; Luzzi, G.; Maisonnier, Ch.; Pecorella, F.; Rager, J. P.; Robouch, B. V.; and Samuelli, M.: Structure of the Dense Plasma Focus, Part I: Numerical Calculations, X-Ray and Optical Measurements. Plasma Physics and Controlled Nuclear Fusion Research — 1971, Vol. I, Int. At. Energy Agency, 1971, pp. 511-521.

5. Maisonnier, Ch.; Gourlan, C.; Luzzi, G.; Papagno, L.; Pecorella, F.; Rager, J. P.; Robouch, B. V.; and Samuelli, M.: Structure of the Dense Plasma Focus, Part II: Neutron Measurements and Phenomenological Description. Plasma Physics and Controlled Nuclear Fusion Research — 1971, Vol. I, Int. At. Energy Agency, 1971, pp. 523-535.

6. Peacock, N. J.; Hobby, M. G.; and Morgan, P. D.: Measurements of the Plasma Confinement and Ion Energy in the Dense Plasma Focus. Plasma Physics and Controlled Nuclear Fusion Research — 1971, Vol. I, Int. At. Energy Agency, 1971, pp. 537-551.

7. Belyaeva, I. F.; and Filippov, N. V.: Location of Fast Deuterons in a Plasma Focus. Nucl. Fusion, vol. 13, no. 6, Dec. 1973, pp. 881-882.

8. Bernstein, M. J.; and Comisar, G. G.: Neutron Energy and Flux Distribution From a Crossed-Field Acceleration Model of Plasma Focus and z-Pinch Discharges. Phys. Fluids, vol. 15, no. 4, Apr. 1972, pp. 700-707.

9. Coudeville, A.; Jolas, A.; Launspach, J.; De Mascureau, J.; and Bernard, A.: Holographic Interferometry and Ruby Laser Scattering on FOCUS Experiments. Bull. American Phys. Soc., ser. II, vol. 18, no. 10, Oct. 1973, p. 1363.

10. Conrads, H.; Cloth, P.; Demmeler, M.; and Hecker, R.: Velocity Distribution of the Ions Producing Neutrons in a Plasma Focus. Phys. Fluids, vol. 15, no. 1, Jan. 1972, pp. 209-211.

11. Lee, J. H.; Shomo, L. P.; and Kim, K. H.: Anisotropy of the Neutron Fluence From a Plasma Focus. Phys. Fluids, vol. 15, no. 12, Dec. 1972, pp. 2433-2438.

12. Potter, D. E.: Numerical Studies of the Plasma Focus. Phys. Fluids, vol. 14, no. 9, Sept. 1971, pp. 1911-1924.

13. Bernstein, Melvin J.: Acceleration Mechanism for Neutron Production in Plasma Focus and z-Pinch Discharges. Phys. Fluids, vol. 13, no. 11, Nov. 1970, pp. 2858-2866.

14. Gary, S. Peter; and Hohl, Frank: Ion Kinematics in a Plasma Focus. Phys. Fluids, vol. 16, no. 7, July 1973, pp. 997-1002.

15. Jalufka, Nelson W.; and Lee, Ja H.: Current Sheet Collapse in a Plasma Focus. Phys. Fluids, vol. 15, no. 11, Nov. 1972, pp. 1954-1958.

16. Toepfer, A. J.; Smith, D. R.; and Beckner, E. H.: Ion Heating in the Dense Plasma Focus. Phys. Fluids, vol. 14, no. 1, Jan. 1971, pp. 52-61.
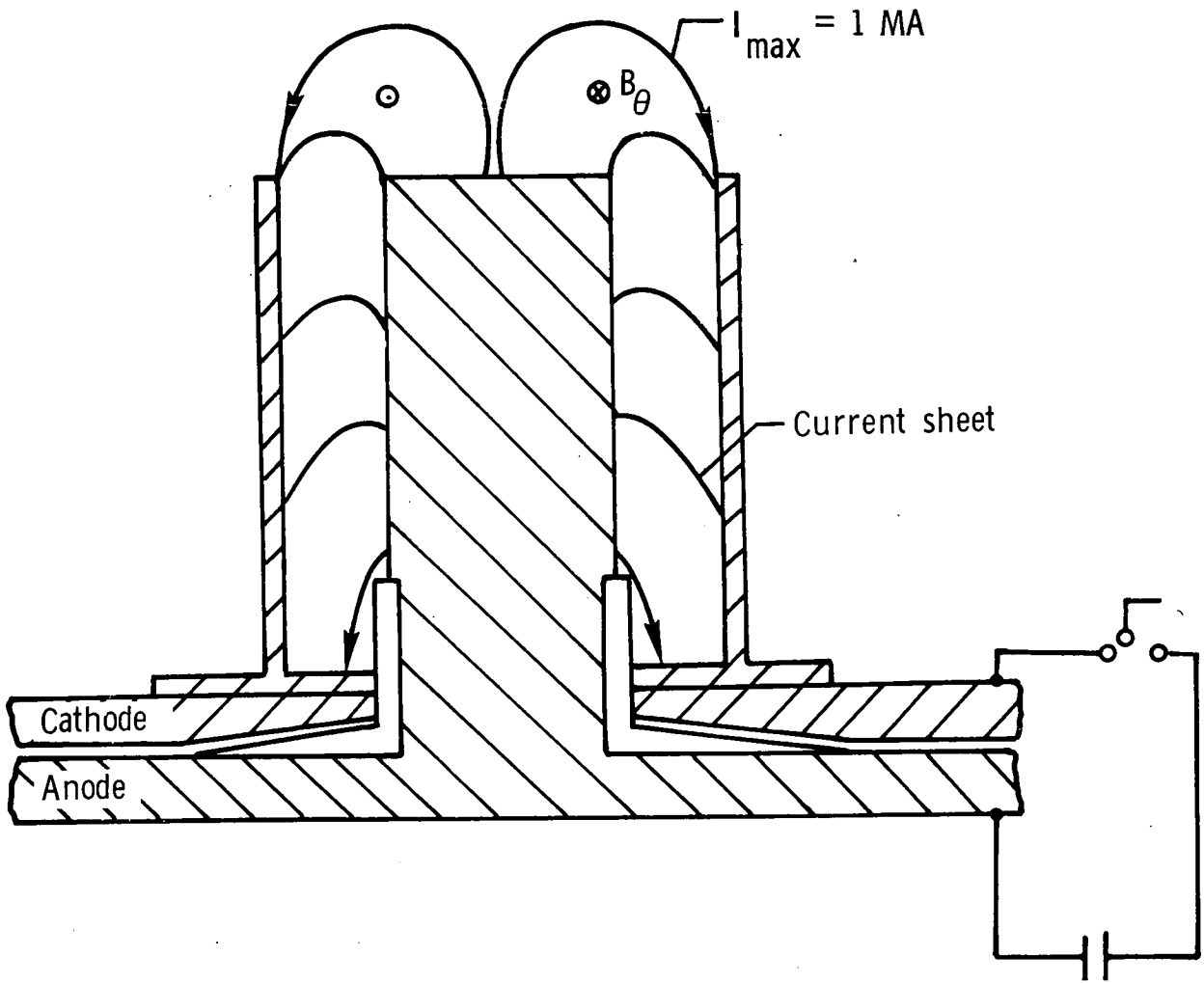
Figure 1.- Cross section through coaxial plasma focus apparatus.

5 cm

-200 -100   0   100   200   300   400

t , ns
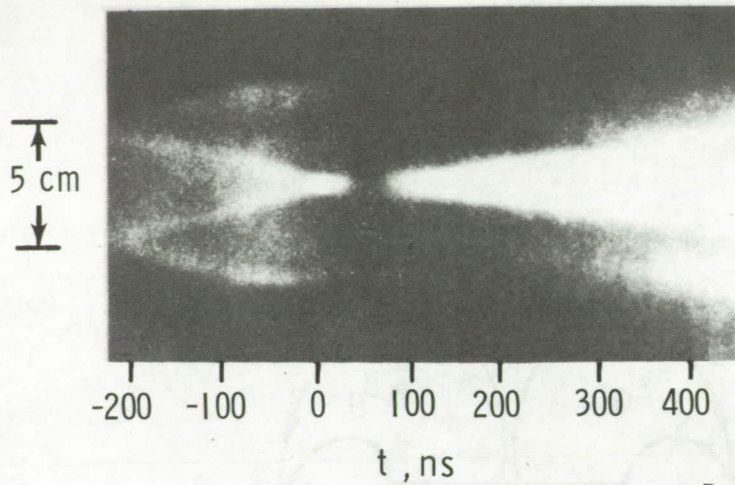
L-74-1161

Figure 2.- Streak photograph of focus formation. (The photograph
displays a region 0.5 cm above the inner electrode, viewed
through a 0.2-cm-wide slit perpendicular to the axis.)

I

E

t (500 ns / div)
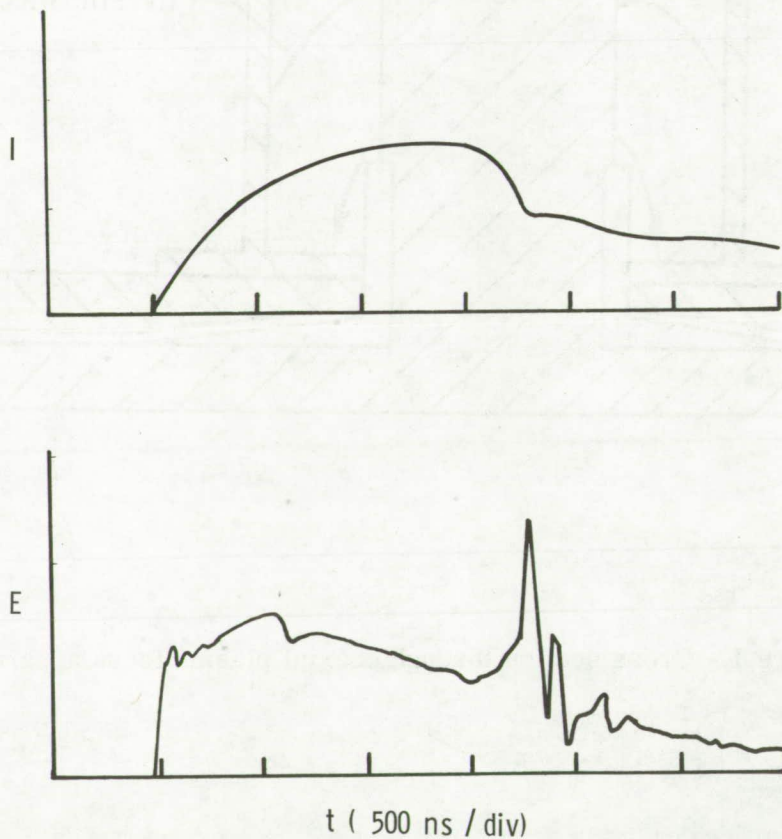
Figure 3.- Traces of typical oscillograms of current and induced electric field.

14
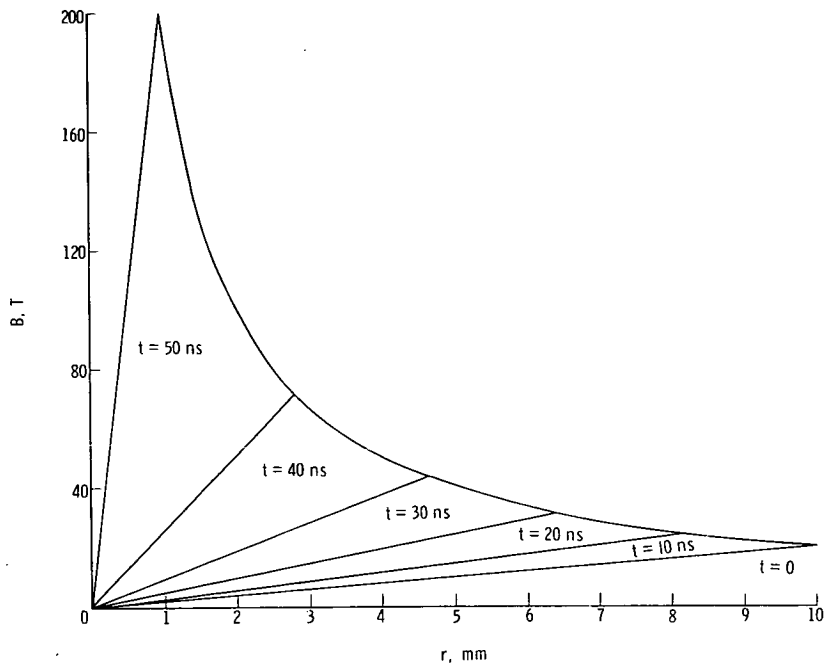
Figure 4.- Radial variation in magnetic field at six times during collapse phase of focus formation.
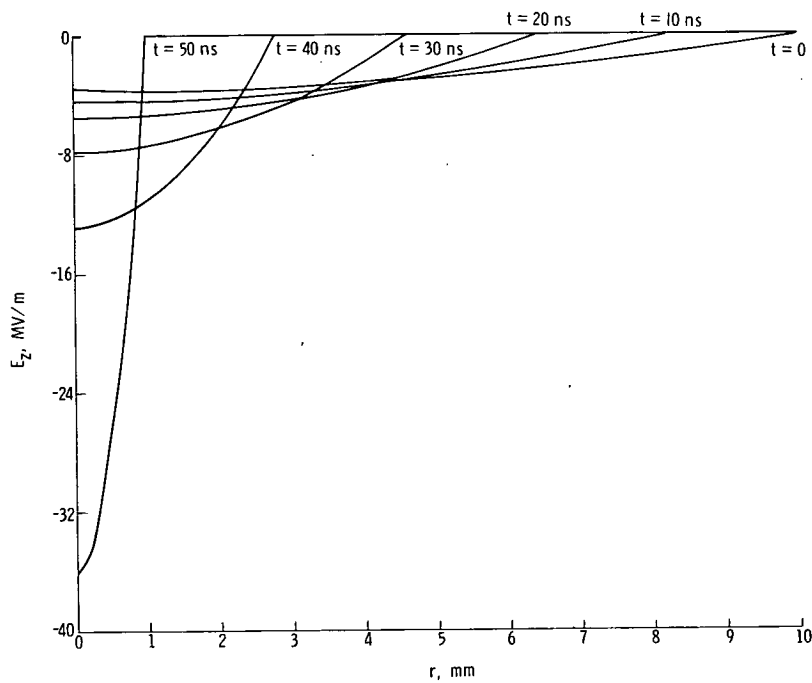
Figure 5.- Radial variation in induced axial electric field at six times during collapse phase of focus formation. (Note that the electric field peaks on the axis and reaches values in excess of 10 MV/m.)

15
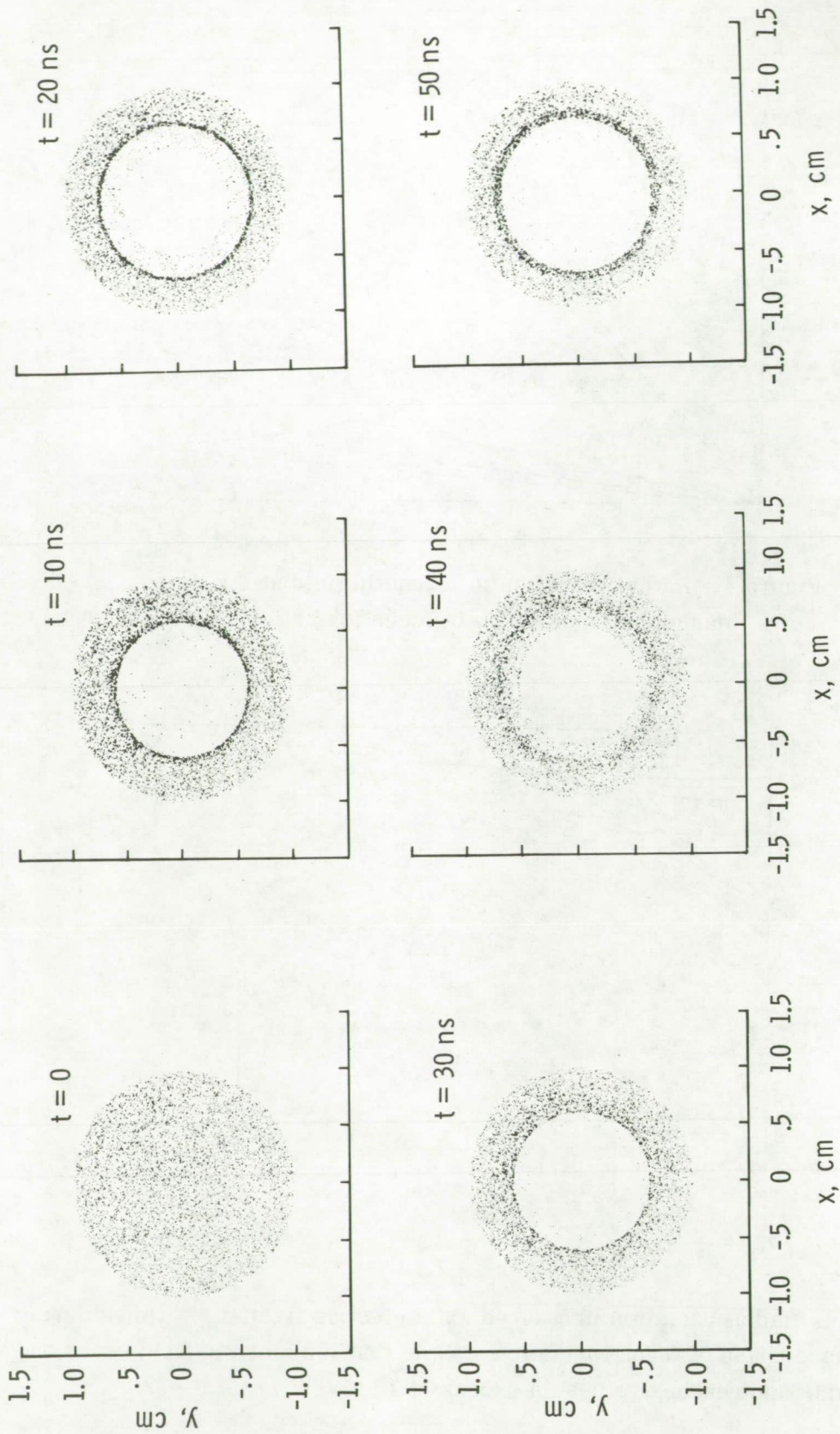
Figure 6.- Evolution of ion distribution during collapse phase of focus formation. (Note that ions are expelled from the central region by the $\vec{E} \times \vec{B}$ drift.)

16
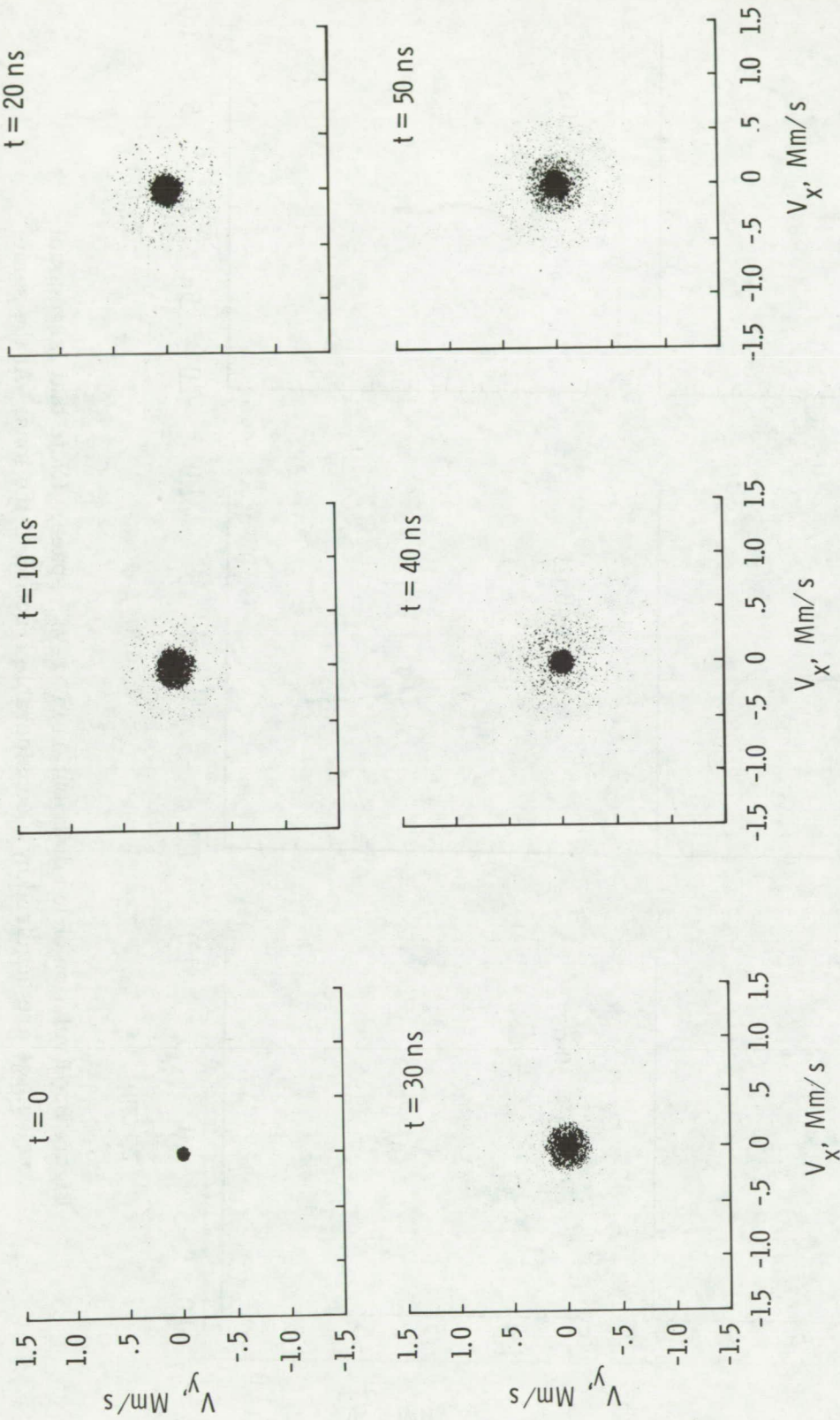
Figure 7.- Evolution of transverse ion velocity distribution during collapse phase. (A fraction of the ions are heated to keV temperatures.)
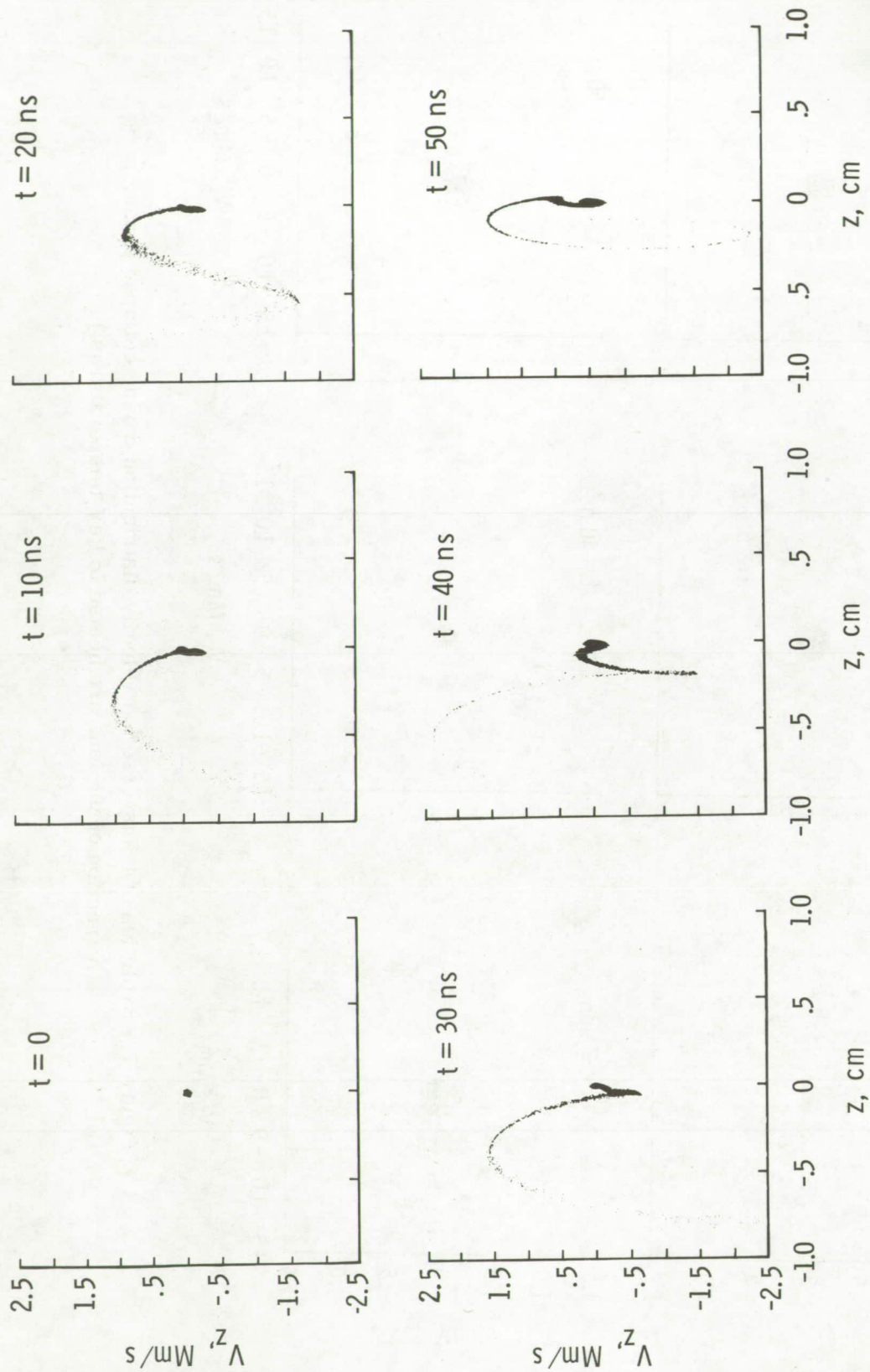
Figure 8.- Evolution of ion distribution in z-V_z space. (Note that large axial velocities are acquired by a considerable fraction of the ions. At the same time the ions are confined near $z = 0$ because of their cyclotron motion.)
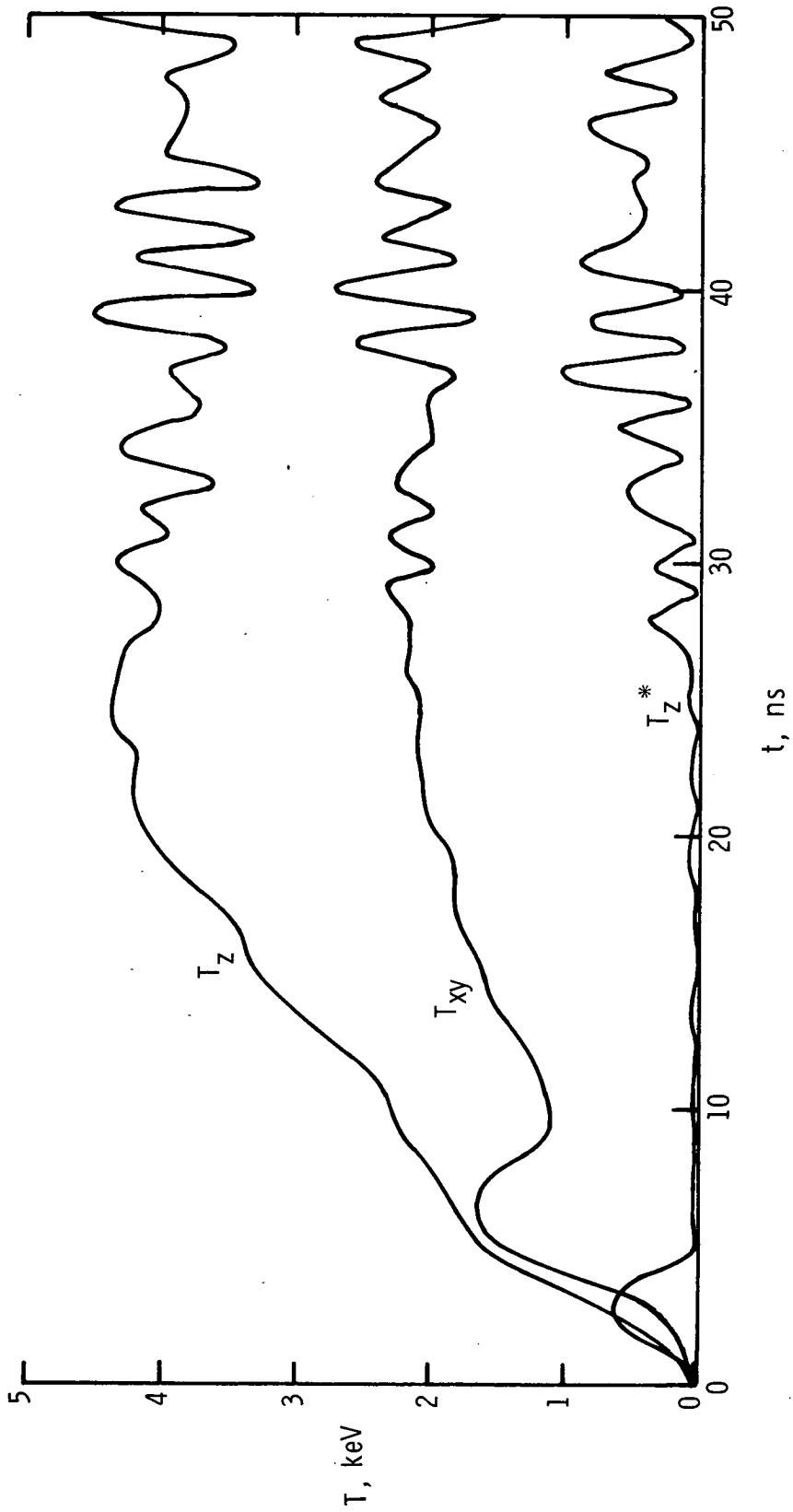
Figure 9.- Evolution of temperature components during collapse phase. (Transverse and axial temperatures reach several keV, whereas the energy in directed beam motion is small.)
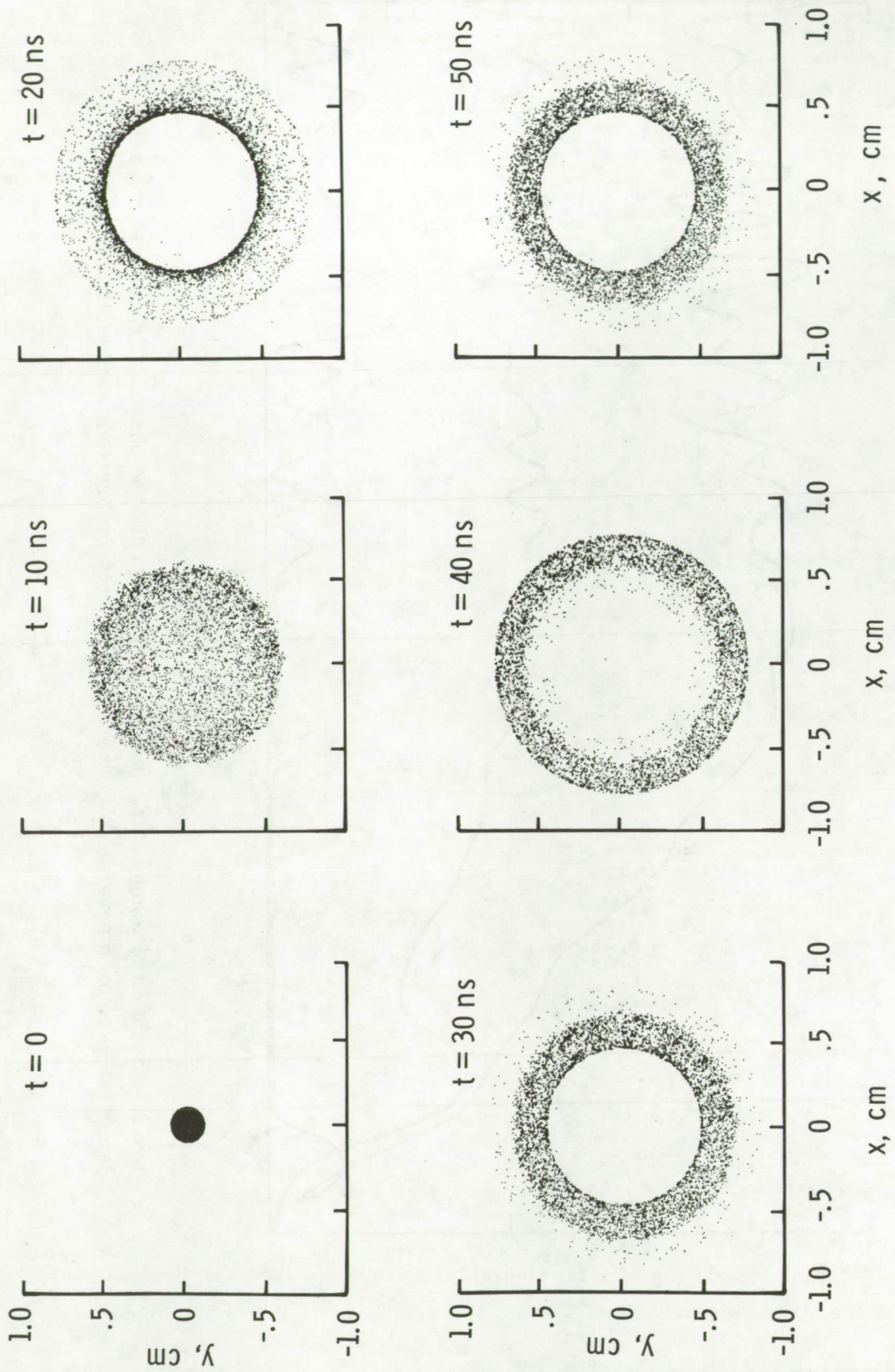
Figure 10.- Evolution of ion distribution during collapse phase. (Initial radius of the circular ion distribution is 1 mm, or one-tenth of that shown in fig. 6.)
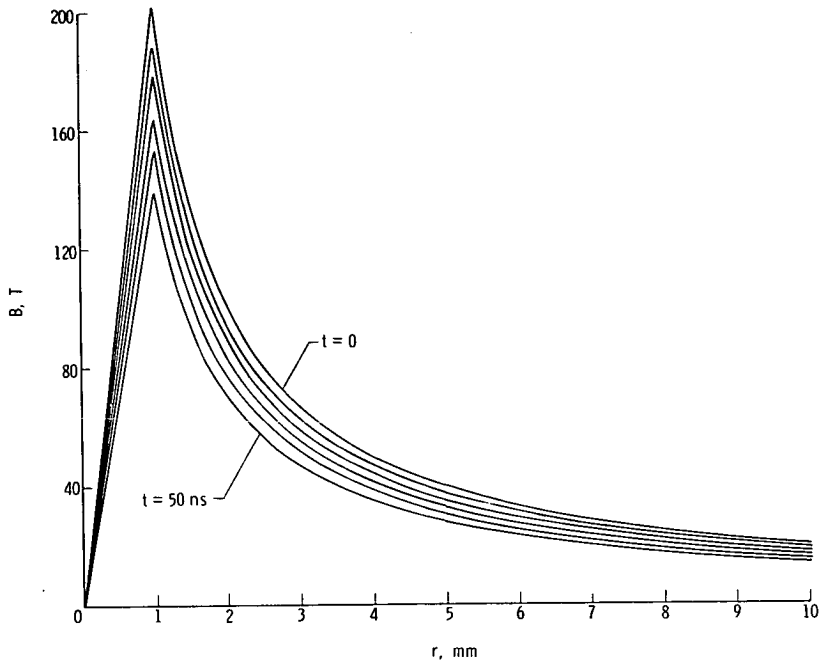
Figure 11.- Radial variation in magnetic field at six times during current-reduction phase of focus formation.
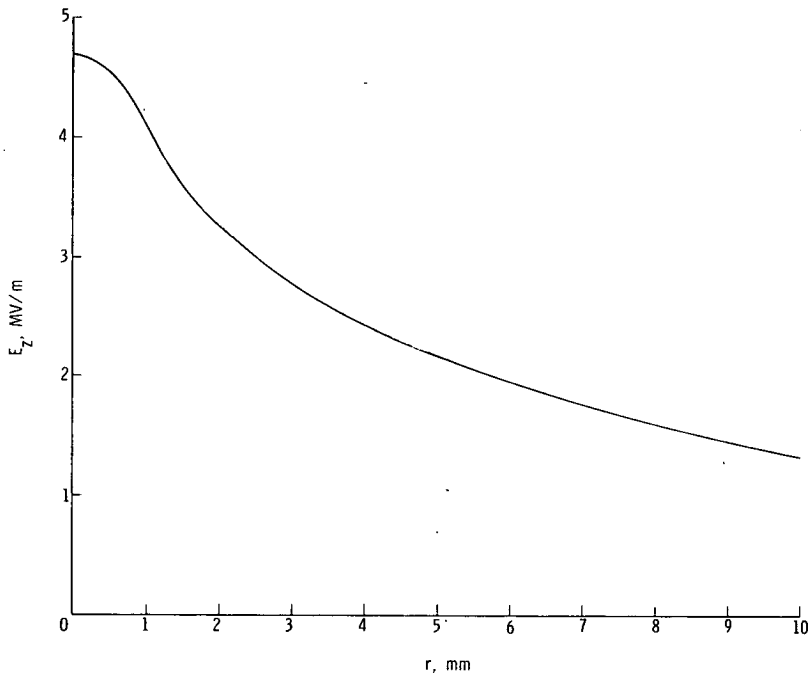
Figure 12.- Radial variation in axial electric field during current-reduction phase. (Note the strong electric field of several megavolts per meter on the axis.)

21
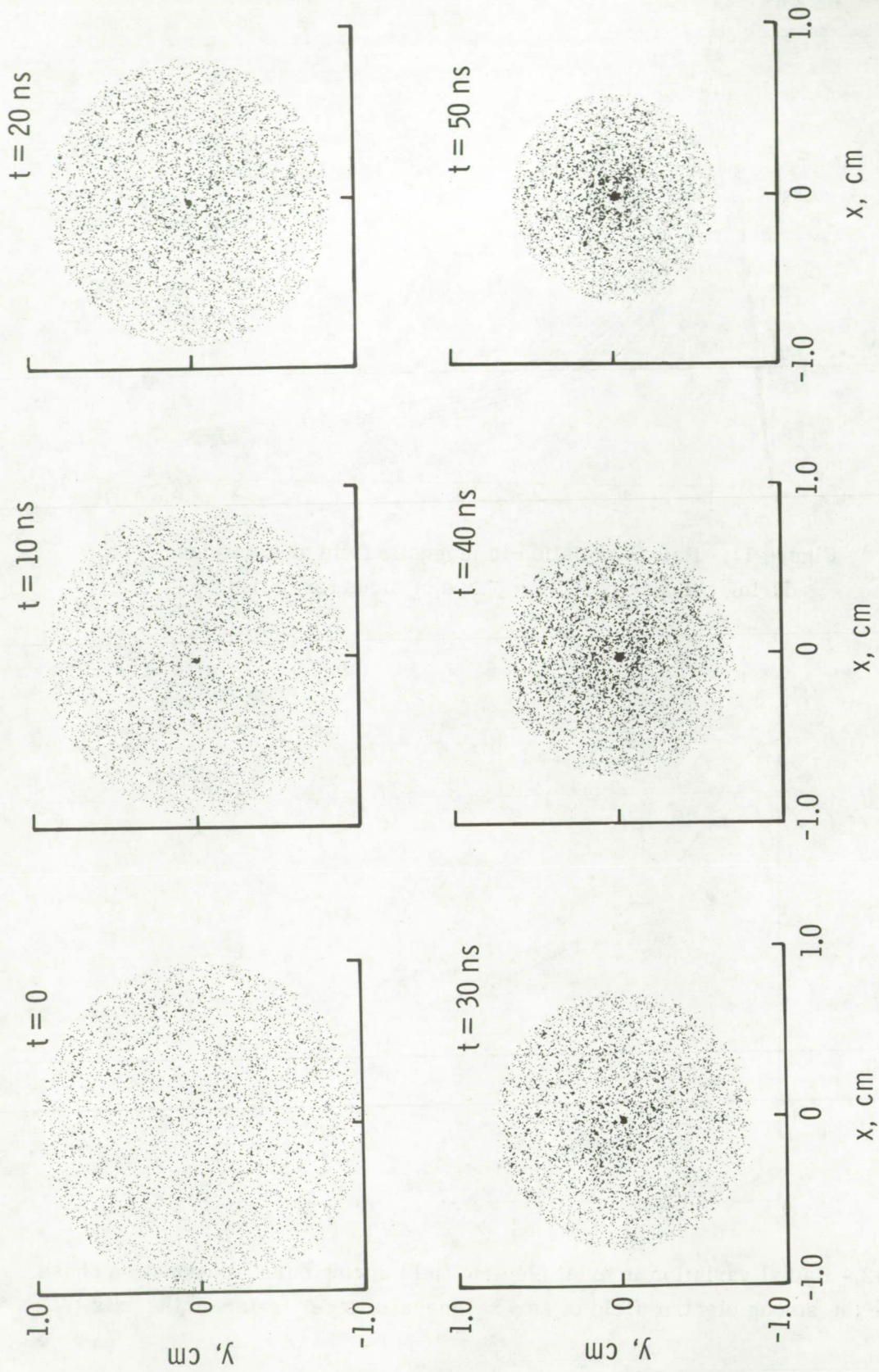
Figure 13.- Evolution of ion distribution during current-reduction phase. (The $\vec{E} \times \vec{B}$ drift now compresses the ion distribution toward the axis, where the ions are accelerated in the z-direction.)

22
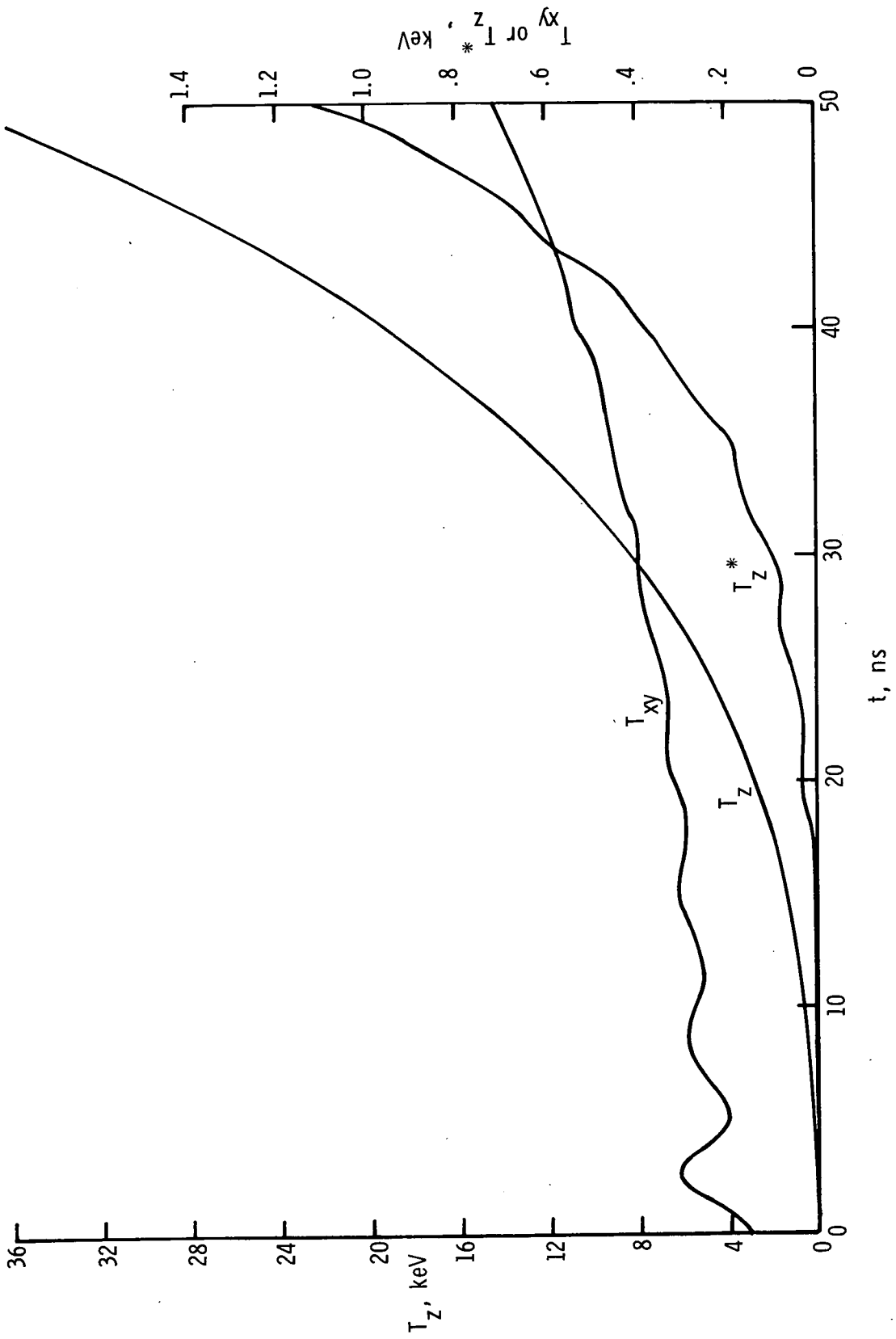
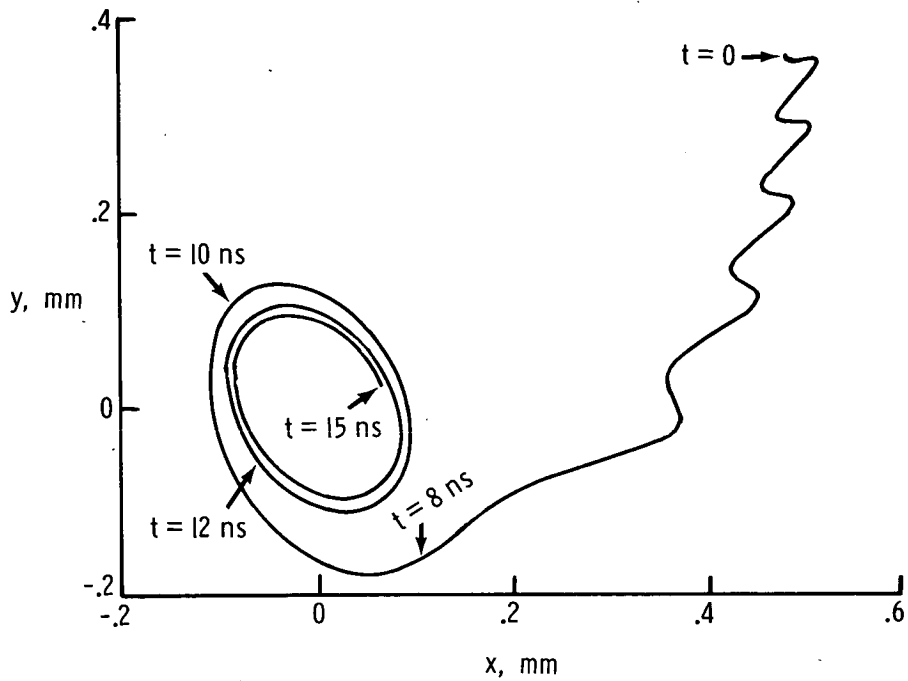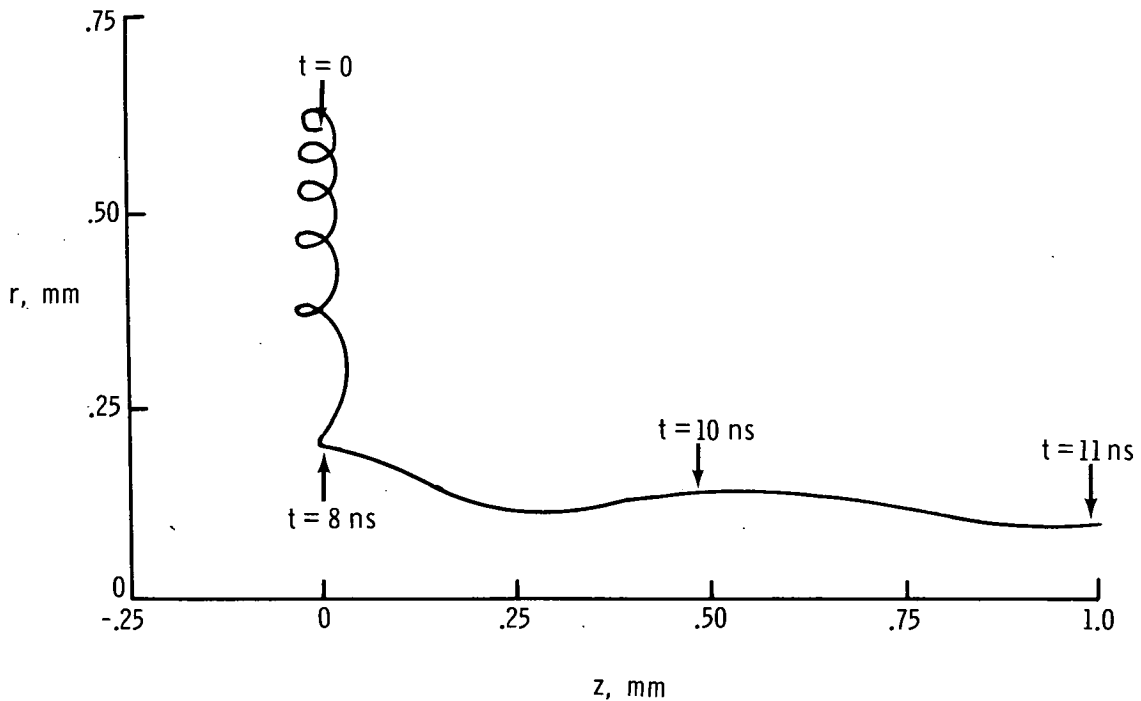Figure 14.- Evolution of ion temperature and energy components during current-reduction phase.
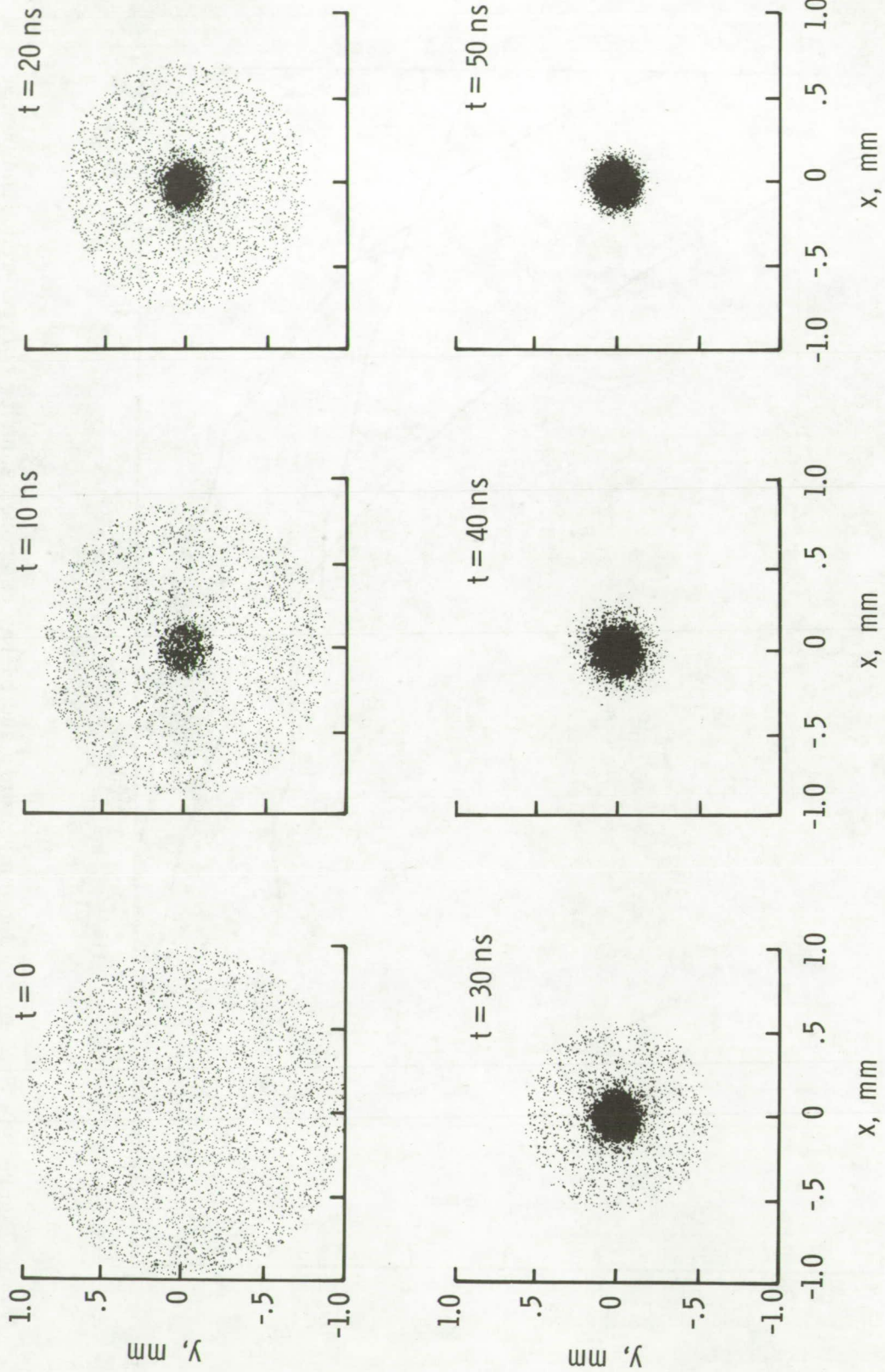
Figure 15.- Evolution of central ion distribution during current-reduction phase. (Note that the initial radius is 1 mm, or one-tenth the radius of the distribution in fig. 13.)

24

(a) Trajectory in x-y space.

(b) Trajectory in r-z space.

Figure 16.- Typical ion trajectory during current-reduction phase. (The ion spirals toward the axis. As it nears the axis it begins to circle the axis and at the same time is accelerated in the z-direction.)
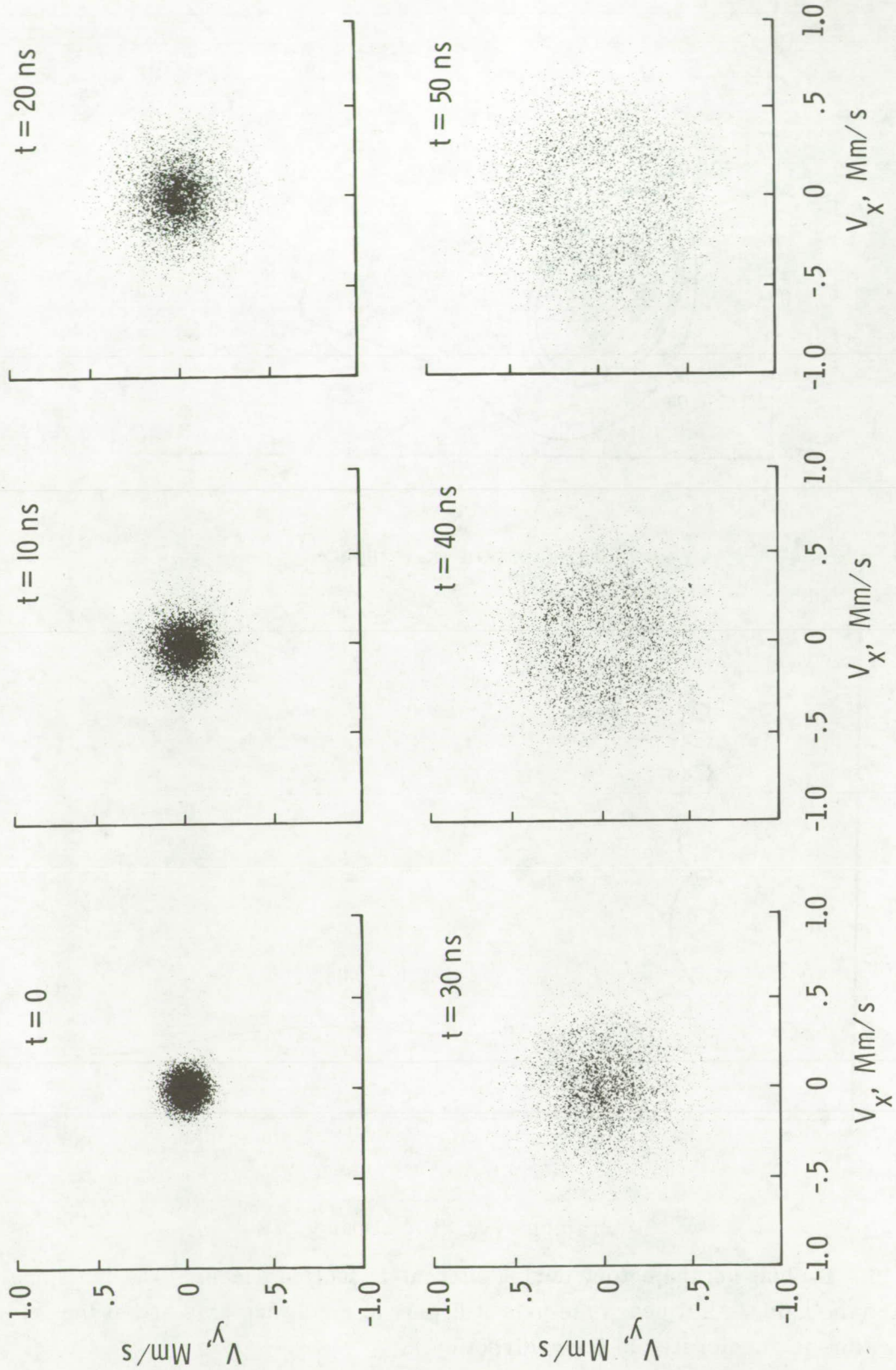
Figure 17.- Evolution of ion velocity distribution during current-reduction phase.
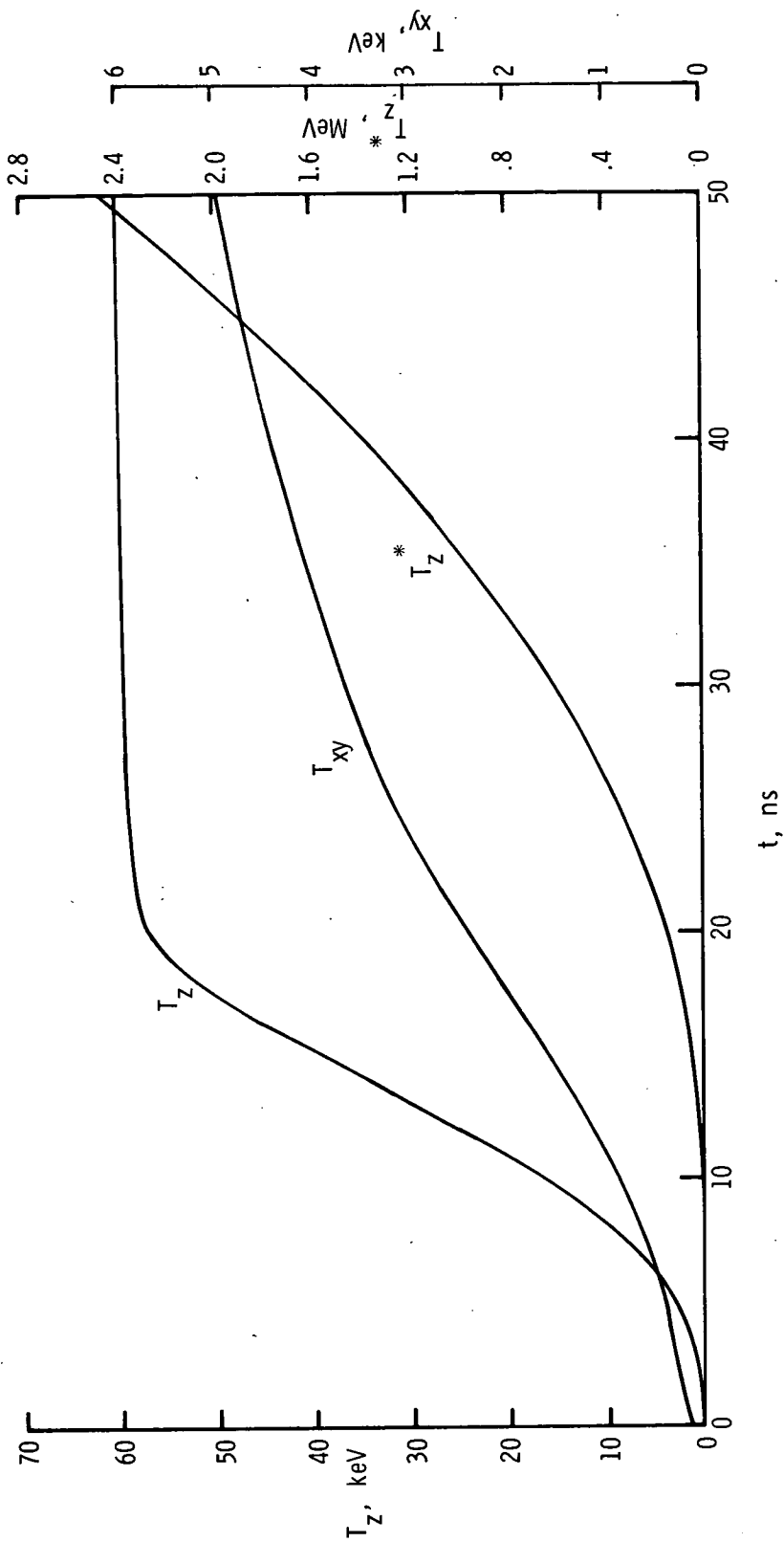
Figure 18.- Evolution of temperature components for central ion distribution during current-reduction phase. (Initial radius of ion distribution is 1 mm.)
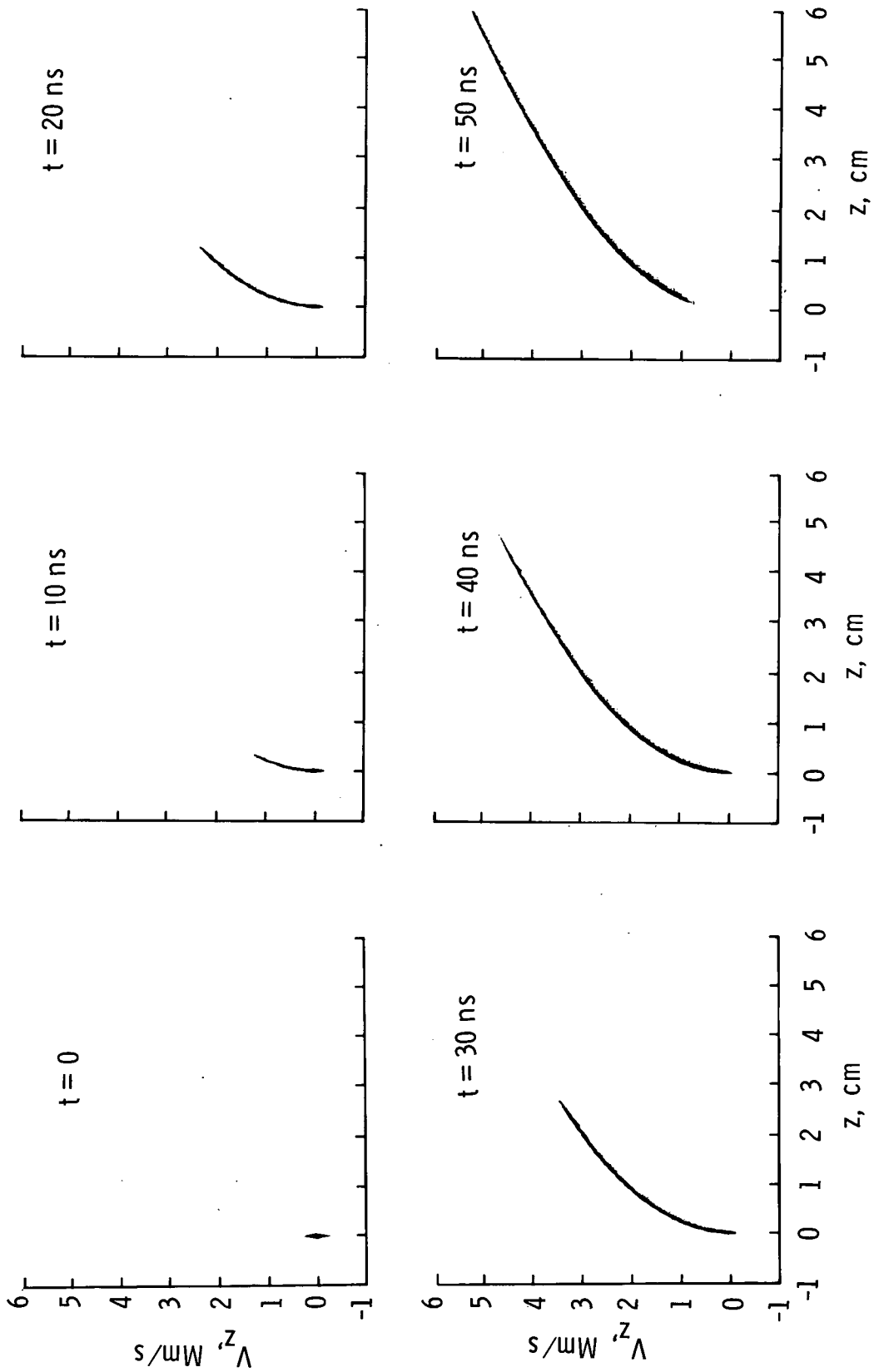
27

Figure 19.- Evolution of central ion distribution in z-V_z space during current-reduction phase.

"The aeronautical and space activities of the United States shall be conducted so as to contribute . . . to the expansion of human knowledge of phenomena in the atmosphere and space. The Administration shall provide for the widest practicable and appropriate dissemination of information concerning its activities and the results thereof."
—NATIONAL AERONAUTICS AND SPACE ACT OF 1958

NASA SCIENTIFIC AND TECHNICAL PUBLICATIONS

TECHNICAL REPORTS: Scientific and technical information considered important, complete, and a lasting contribution to existing knowledge.

TECHNICAL NOTES: Information less broad in scope but nevertheless of importance as a contribution to existing knowledge.

TECHNICAL MEMORANDUMS: Information receiving limited distribution because of preliminary data, security classification, or other reasons. Also includes conference proceedings with either limited or unlimited distribution.

CONTRACTOR REPORTS: Scientific and technical information generated under a NASA contract or grant and considered an important contribution to existing knowledge.

TECHNICAL TRANSLATIONS: Information published in a foreign language considered to merit NASA distribution in English.

SPECIAL PUBLICATIONS: Information derived from or of value to NASA activities. Publications include final reports of major projects, monographs, data compilations, handbooks, sourcebooks, and special bibliographies.

TECHNOLOGY UTILIZATION PUBLICATIONS: Information on technology used by NASA that may be of particular interest in commercial and other non-aerospace applications. Publications include Tech Briefs, Technology Utilization Reports and Technology Surveys.

Details on the availability of these publications may be obtained from:

SCIENTIFIC AND TECHNICAL INFORMATION OFFICE

NATIONAL AERONAUTICS AND SPACE ADMINISTRATION
Washington, D.C. 20546